

Could Crop Height Affect the Wind Resource at Agriculturally Productive Wind Farm Sites?

Brian Vanderwende¹ · Julie K. Lundquist^{1,2}

Received: 5 February 2015 / Accepted: 20 October 2015 / Published online: 7 November 2015
© The Author(s) 2015. This article is published with open access at Springerlink.com

Abstract The collocation of cropland and wind turbines in the US Midwest region introduces complex meteorological interactions that could influence both agriculture and wind-power production. Crop management practices may affect the wind resource through alterations of land-surface properties. We use the weather research and forecasting (WRF) model to estimate the impact of crop height variations on the wind resource in the presence of a large turbine array. A hypothetical wind farm consisting of 121 1.8-MW turbines is represented using the WRF model wind-farm parametrization. We represent the impact of selecting soybeans rather than maize by altering the aerodynamic roughness length in a region approximately 65 times larger than that occupied by the turbine array. Roughness lengths of 0.1 and 0.25 m represent the mature soy crop and a mature maize crop, respectively. In all but the most stable atmospheric conditions, statistically significant hub-height wind-speed increases and rotor-layer wind-shear reductions result from switching from maize to soybeans. Based on simulations for the entire month of August 2013, wind-farm energy output increases by 14 %, which would yield a significant monetary gain. Further investigation is required to determine the optimal size, shape, and crop height of the roughness modification to maximize the economic benefit and minimize the cost of such crop-management practices. These considerations must be balanced by other influences on crop choice such as soil requirements and commodity prices.

Keywords Agriculture · Iowa · Roughness length · Wind-farm parametrization · Weather research and forecasting model

✉ Brian Vanderwende
vanderwb@colorado.edu

¹ Department of Atmospheric and Oceanic Sciences, University of Colorado, Boulder, CO 80309, USA

² National Renewable Energy Laboratory, Golden, CO 80401, USA

1 Introduction

The abundance of realized and potential wind-power resources in the agriculture-intensive Midwest and Great Plains regions of the USA stimulates discussion on the interactions between wind farms and cropland (Baidya Roy and Traiteur 2010; Rajewski et al. 2013). Such interaction is already a reality in states such as Texas, Iowa, Illinois, Oklahoma, and Kansas, where wind power has become established and agriculture has long been a way of life. Future projections, such as the *20% wind energy by 2030* report by the US Department of Energy (2008), recognize the tremendous wind potential of the “Bread Basket” wheat-producing Great Plains states and the “Corn Belt” maize-producing Midwest states; these studies suggest the aforementioned regions will play a dominant role in the evolving USA energy landscape. By necessity, most wind farms in these states are located on existing cropland. Therefore, wind turbines have the potential to alter crop growth through the modification of surface fluxes of heat and moisture (Zhou et al. 2012; Harris et al. 2014). Conversely, crop growth and harvesting cycles modify local surface properties, the effects of which can influence the wind resource aloft (e.g., changes to the rotor-layer wind speed, wind shear, and vertical momentum fluxes).

Long before wind power became an important contributor to the energy market, the impacts of the land surface on atmospheric flow were an intense area of study. Landscape features (such as crops) can affect the momentum field aloft through frictional surface drag. This process is often modelled using an aerodynamic roughness length, z_0 . Large roughness elements—buildings, trees, and wind turbines, to name a few—affect the wind profile over a larger vertical extent, and therefore have larger roughness lengths than smaller roughness elements. The spatial configuration of the elements also determines the roughness length: a dense, regular grid of elements affects air motions differently than sparse, irregularly-arranged structures. When one roughness regime gives way to another, the flow near the ground gradually adjusts to the new surface characteristics. This process is often represented mathematically by local internal boundary layers (IBLs), which grow vertically downstream of a roughness boundary (Elliott 1958; Panofsky and Townsend 1964; Townsend 1965; Peterson 1969; Blom and Wartena 1969).

The wide range of observed roughness lengths presents an additional challenge when using numerical modelling to simulate land–atmosphere interactions. At synoptic and mesoscale grid resolutions, roughness is almost always inhomogeneous across any given grid cell. It therefore becomes necessary to parametrize this inhomogeneity in the model representation of the land surface. One solution is the concept of the effective roughness length, in which a homogeneous roughness value is chosen that results in atmospheric wind profiles and/or surface stresses that match, as closely as possible, the values that would be obtained by averaging the flow field over the actual heterogeneous surface. Many approaches to formulate effective roughness lengths have been proposed, ranging from simple averages (Fiedler and Panofsky 1972) to the concept of a blending height (Mason 1988; Claussen 1990; Goode and Belcher 1999; Bou-Zeid et al. 2004), the height at which individual roughness perturbations blend into a spatially homogeneous flow field (Wieringa 1976). Later references to roughness and to z_0 imply an effective roughness length.

As interest in wind power grows, the effects of wind-farm development on regional and global climate have been simulated by modifying the roughness lengths used in atmospheric models (Ivanova and Nadyozhina 2000; Keith et al. 2004; Kirk-Davidoff and Keith 2008; Barrie and Kirk-Davidoff 2010; Wang and Prinn 2010, 2011). These studies attempt to quantify the aggregate effect of turbines on the large-scale wind field, boundary-layer temperature and precipitation. Such simulations have also been used to suggest physical limits to the global

wind-power resource that result from momentum extraction by large quantities of expansive wind farms (Jacobson and Archer 2012; Adams and Keith 2013). There are pitfalls to the roughness approach, however: uncertainty in choosing an appropriate roughness value, unrealistic representations of boundary-layer profiles (Fitch et al. 2013b), and potentially erroneous values of wind-turbine density (Adams and Keith 2013). The modification of roughness lengths to represent wind turbines also prevents the simulation of the effect of natural roughness variability on wind-farm output, which is fundamental to the questions posed herein.

Fortunately, it is also possible to simulate wind farms at large scales by using elevated drag parametrizations to represent the extraction of momentum and production of turbulent kinetic energy (TKE) at turbine-rotor level heights. Research efforts utilizing this method include: Baidya Roy et al. (2004), who used a constant momentum sink and TKE source, Blahak et al. (2010) and Baidya Roy (2011), who based the fraction of energy extracted on the power coefficient of a commercial turbine, and Fiedler and Bukovsky (2011), Fitch et al. (2012), and Adams and Keith (2013), who used velocity-dependent thrust and power coefficients to partition extracted power into electricity and turbulence. Jacobson and Archer (2012) also use the latter approach, but neglect direct TKE production in favour of an implicit source resulting from the wind shear in the wake layer. Fitch et al. (2013b) demonstrated the benefits of using an elevated drag approach over a roughness length modification; simulated diurnal cycles of wind-speed deficit, TKE, and temperature change were reversed between the two approaches, with the elevated drag approach matching the few studies of wind-farm wakes currently available (Christiansen and Hasager 2005; Baidya Roy and Traiteur 2010; Zhou et al. 2012). Though the aforementioned studies yield insight into wind-turbine impacts on the atmospheric diurnal cycle, our knowledge of interactions between wind farms and the land surface remains primitive.

In this study, we use a numerical weather prediction model to test the hypothesis that wind-farm power output can be enhanced through the selective planting of lower-roughness crops on the underlying land surface. We use an elevated drag wind-farm parametrization (WFP), which allows for the modification of roughness in the presence of a representative wind farm. In Sect. 2, we describe the model domain and physics, the method used to represent roughness, and the WFP. The impact of switching from maize to soybeans on the wind profile at the centre of the hypothetical wind farm is discussed in Sect. 3, and we analyze the streamwise wind-speed changes for four defined stability classes in Sect. 4. A simple economic analysis is performed and a short discussion of the roughness effect in the context of future turbine trends is provided within Sect. 5. Finally, we discuss limitations in our analysis and potential future avenues of research in Sect. 6.

2 Model Configuration and Methods

To simulate large-scale-roughness impacts on wind turbines, an atmospheric model with an elevated-drag wind-farm representation is required. Version 3.4.1. of the weather research and forecasting (WRF) model is used, which includes the WFP (hereafter referred to as the WRF-WFP model) described in Fitch et al. (2012). The WRF model is a collaborative effort between the National Center for Atmospheric Research and the geoscience community, built with a modular design that allows for multiple solver, physics, data, and grid options. The advanced research WRF model dynamical core features a fully-compressible, non-hydrostatic, time-split integration solver with an Arakawa-C staggered horizontal grid and a stretched terrain-following vertical grid (Skamarock et al. 2008).

Although a very limited set of observations is available for field validation of this model, initial investigations have demonstrated its ability to qualitatively reproduce measured power

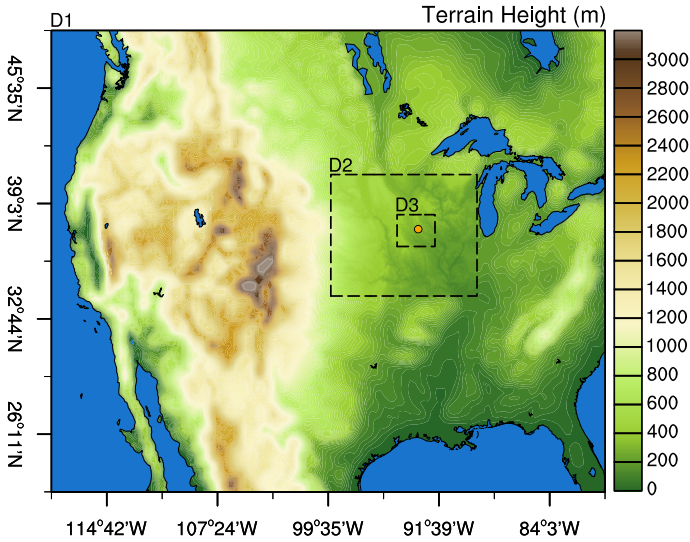


Fig. 1 The spatial extent and terrain heights (m) of the three model domains. The orange dot represents the CWEX 2013 field site and the location of the hypothetical wind farm used in this study

deficits at the Horns Rev offshore wind farm (Jiménez et al. 2014). The WRF-WFP model's performance over a diurnal cycle has been explored by Fitch et al. (2013a), in which the model produced near-surface temperature perturbations similar to those from large-eddy simulations of wind farms impacts on flow. Unlike simpler surface-based roughness representations of wind farms, the WRF-WFP model correctly replicates the elevated vertical location of the wind-farm momentum deficit as well as secondary flow features such as near-surface speed-up in stable conditions (Fitch et al. 2013b). The WRF-WFP model is now being used by the community to address broader scientific questions, such as a recent study analyzing the impact of European wind farms on regional climate (Vautard et al. 2014).

The model domain configuration utilized herein consists of three two-way nested domains with horizontal resolutions of 31.25, 6.25, and 1.25 km, respectively. All three domains feature 60-level vertical grids, with approximately 15-m cell spacing from the surface to 120 m, a typical maximum height for a modern utility-scale turbine. The vertical grid spacing then progressively stretches from the height of 120 m to the model top. Our simulations utilize the rapid radiative transfer model longwave and Dudhia shortwave radiation schemes, the WRF model single-moment six-class microphysics scheme, the Noah land-surface model, and the MYNN planetary boundary-layer (PBL) scheme. The Grell three-dimensional cumulus parametrization is used to simulate convection on the two coarser domains. ERA-interim boundary and initial condition data are used to drive the weather in the outer domain. These choices for physics options and boundary conditions have been selected based on the simulations of Vanderwende et al. (2015). The coarsest domain spans the entire continental USA while the finest domain roughly encompasses the State of Iowa (Fig. 1). In addition to being the largest US producer of both maize and soybeans, Iowa is also a leader in the early adoption of wind energy. In 2013, power producers in Iowa met over 27 % of the state's electricity needs with wind farms (American Wind Energy Association 2014). Therefore, Iowa is a natural location to study crop–wind interactions.

Furthermore, central Iowa is the location of the crop–wind energy experiment (CWEX), a multi-year field campaign designed to investigate turbine–crop interactions (Rajewski et al.

Table 1 A summary of the specifications for the turbine model used in the WRF model wind-farm parametrization model

Turbine specifications	
Manufacturer	Vestas
Type	V90
Capacity	1.8 MW
Cut-in speed	4 m s ⁻¹
Rated speed	12 m s ⁻¹
Cut-out speed	25 m s ⁻¹
Hub height	80 m
Rotor diameter	90 m

2013; Rhodes and Lundquist 2013). The site features gentle, mostly flat terrain and heterogeneous roughness resulting from a patchwork arrangement of field management. The 2013 deployment, which spanned the months of July and August, featured three WINDCUBE™ V1 lidar systems, a WINDCUBE™ 200S scanning lidar, and seven surface-flux stations. Additional details of the deployment are provided in Lundquist et al. (2014). These observations were used in Vanderwende et al. (2015) to evaluate the ability of the WRF model to simulate observed nocturnal low-level jets (LLJs). The skill demonstrated by the WRF model in simulating such complex phenomena at this site justifies its use in the present study.

Low-level flow in summer at the CWEX site is typically driven by a synoptic weather pattern that features broad south-south-westerly flow circulating around a large sub-tropical anticyclone to the south-east. The LLJ punctuates this weather regime, accelerating the southerly winds aloft at night (Bonner 1968). This general pattern is occasionally interrupted by frontal passages from the north, with associated northerly winds and unsettled weather. All of these weather conditions were observed during the CWEX 2013 field campaign (Vanderwende et al. 2015).

2.1 Configuration of the Simulated Wind Farm

We use the WRF-WFP model to represent a hypothetical wind farm with a regular square layout at the CWEX location within the finest model domain. The wind farm consists of 121 1.8-MW Vestas V90 turbines, with rows and columns spaced six rotor-diameters (540 m) apart to avoid wake influences among the turbines. The rated capacity (218 MW) of this modelled wind farm lies within the range of existing wind farms in central Iowa, though we do not recreate the real-world configuration at the CWEX site, which features irregular geometry and a larger footprint. The 1.8-MW V90 turbines, specifications for which are listed in Table 1, are designed for low-to-medium wind conditions. The operating range of the turbine is well suited to the August 2013 wind fields simulated by the WRF model, as shown by the expected power curve and modelled wind-speed distribution in Fig. 2. Five wind-speed bins are defined, indicating the relative sensitivity of turbine power output to changes in the wind speed. For example, wind-speed changes in the 6–10 m s⁻¹ range have the strongest impact on turbine output. Note that only rarely do wind speeds exceed 12 m s⁻¹, the magnitude at which rated power is reached.

2.2 Using Roughness to Represent the Two Crop Choices

The two most prevalent crops in Iowa are maize and soybeans, each of which has distinct characteristics when mature (in their reproductive growth stage). Therefore, these plants rep-

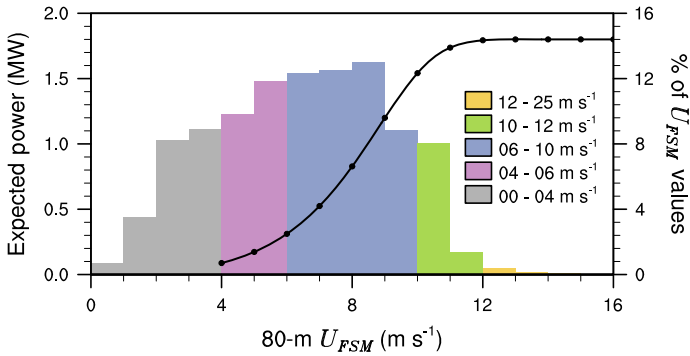


Fig. 2 The power curve for the 1.8-MW Vestas V90 turbines used. The distribution of simulated 80-m (hub height) wind speeds (m s^{-1}) for August 2013 is also shown by the coloured bars. The colours represent wind-speed bins designed to highlight varying sensitivities of the power output–wind-speed changes

resent practical cases for estimating the impact of crop choice on wind resources. To simplify the analysis, we use only z_0 values to represent the different crop choices for 1-month-long simulations spanning August 2013. As both plants are typically mature during this month, the choice of z_0 as our imposed parameter results in a steady-state crop representation. The inclusion of moisture and evapotranspiration considerations for each crop would add a time-varying complication, likely requiring the use of an extensive observational dataset for validation.

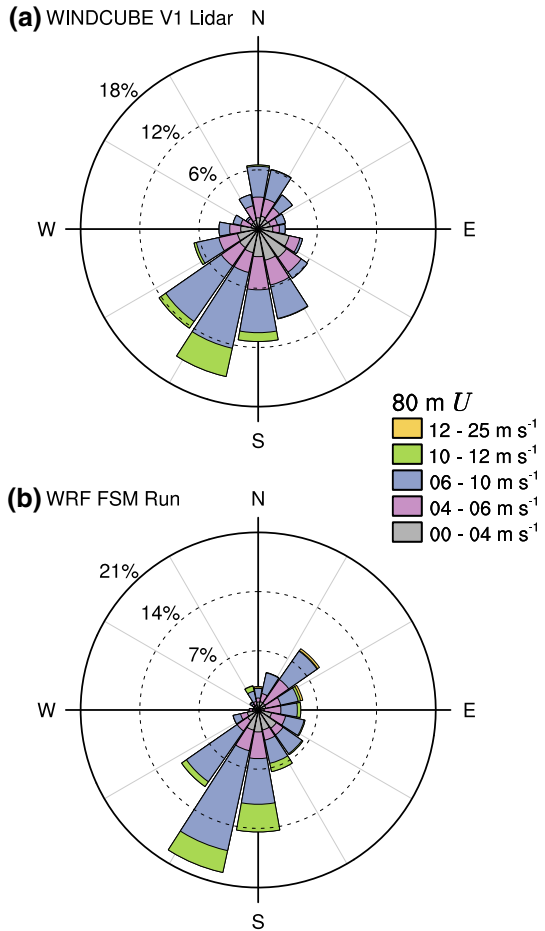
For estimates of the effective roughness lengths associated with each crop, we turn to the Davenport roughness classification (Wieringa 1992). Using the descriptions provided in the classification scheme, we assign maize to the *rough* category ($z_0 = 0.25 \text{ m}$) and soybeans to the *roughly open* category ($z_0 = 0.1 \text{ m}$). These values correspond to those of high and low crops, as described in the classification, and are representative of the ranges of observed roughness values (from studies such as Hicks and Wesely 1981; Wieringa 1993; Hansen 1993) for each crop surface (0.05–0.1 m for soybeans, 0.17–0.74 m for maize). Note that these values are used to simulate mature crops only; analyses at different periods of the crop growth cycle would require different representative roughness lengths.

2.3 Roughness Patch Considerations

Many exploratory modelling studies of wind-farm impacts and interactions use unrealistically large features to first establish the plausibility of a given phenomenon. Here, however, if the area over which the crop change is made (henceforth referred to as the roughness patch) is too large, then any possible power increase would be negated by the impracticality of managing land use over such a region.

Fortunately, we need not make a random guess as to an appropriate patch size. Mason (1988) suggested that the boundary layer should be in local vertical equilibrium with surface roughness up to height of $L/200$, where L is the horizontal fetch over the roughness patch. Using this relationship, we find that a fetch of 25 km over the roughness patch is required to allow the effects of surface drag to propagate up to the top of the turbine–rotor layer (125 m). The distribution of hub-height wind directions in August 2013, shown in Fig. 3, indicates frequent south-south-westerly winds in both our lidar observations and WRF model simulations. The simulated winds mostly match the observed south-westerly-dominated distribution of wind directions. Small inaccuracies in simulated LLJs produce less spread in south-westerly

Fig. 3 The distribution of simulated 80-m wind speeds (m s^{-1}) and directions for August 2013, from **a** a WINDCUBE™ V1 lidar, and **b** the WRF model freestream maize surface simulation. As in Fig. 2, the wind-speed bins are derived from the slope of the turbine power curve



wind directions in the WRF model output. Additionally, northerly wind directions were shifted to the north-east in the model run, largely due to erroneous positioning of a stationary front on 12 August. However, most inflow angles are accurately represented during the month, which justifies modifying the upwind roughness in those directions. To be conservative, we use a symmetric square roughness patch centred on the wind farm, yielding a fetch between 25 and 40 km depending on the exact inflow angle.

The spatial arrangement of the wind farm and the roughness patch is illustrated in Fig. 4, which provides a close-up view of the innermost domain. The wind farm, indicated by the red square, measures $6.3 \times 6.3 \text{ km}^2$, while the roughness patch, indicated by the blue square, measures $56.3 \times 56.3 \text{ km}^2$.

2.4 Summary of the Simulation Suite

In all, 4-month-long simulations are produced spanning August 2013. (Recall, August was chosen as the month with the most significant differences between the heights and therefore roughness lengths of the crops.) The first two simulations compare the effect of maize versus soybean surface roughness in an atmosphere undisturbed by the presence of a wind farm.

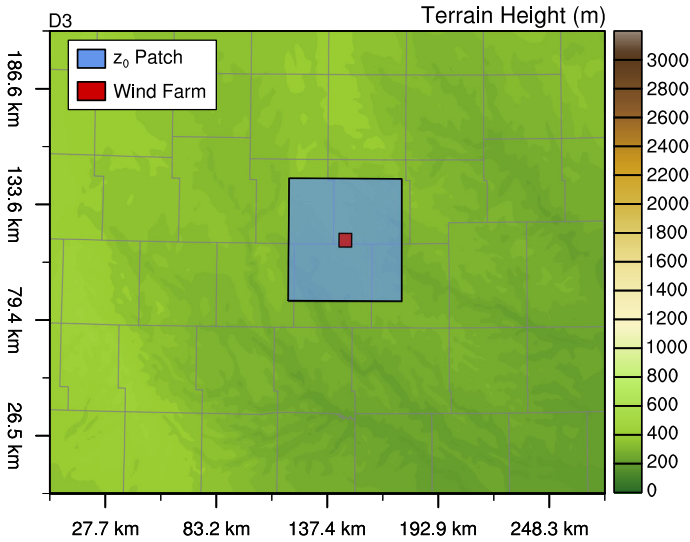


Fig. 4 A closer look at the coverage and terrain height of the innermost model domain, highlighting the spatial extent of both the wind farm (red) and the roughness patch (blue). The grey lines represent county borders within Iowa

We use the term “freestream” to exclusively represent this undisturbed state throughout the remainder of this paper, i.e., a reference simulation with no wind-farm obstruction. The second set of simulations represent this crop effect in the presence of the hypothetical wind farm, which itself modifies winds aloft by extracting momentum from the flow and generating additional turbulence. In all figures, data from these four simulations are identified with the following abbreviations: FSM for freestream maize, FSS for freestream soybeans, WFM for wind-farm maize, and WFS for wind-farm soybeans. This suite of simulations allows us to determine whether the wind farm contributes to and/or inhibits the roughness effect in a significant way, and whether or not the effect of the surface is still distinguishable in the presence of a wind farm.

3 Effects of Crop Selection on the Local Wind Profile

In both the freestream and the wind-farm sets of simulations, changing from a maize to soybean surface roughness results in an increase in rotor-layer wind speeds and a decrease in rotor-layer TKE. Profiles of these changes are shown in Fig. 5 for one grid cell in the centre of the wind farm. Changes forced by crop selection are largest at the surface and slowly decay aloft. In the rotor layer, median wind-speed increases range from 0.2 to 0.35 m s^{-1} , while median TKE (e) decreases are between 0.01 and $0.04 \text{ m}^2 \text{ s}^{-2}$. Given that the finest domain uses a 1.25-km resolution, turbulence is not resolved by the model grid but rather estimated by the MYNN PBL scheme. Despite this potential source of error, any changes to TKE production are important, as turbulence can affect turbine power output and increase stresses on the turbine structure (e.g., Eggers et al. 2003; Kelley 2011).

Differences between the freestream and wind-farm results are generally small, with the largest changes in the rotor layer as would be expected. The presence of the wind farm reduces

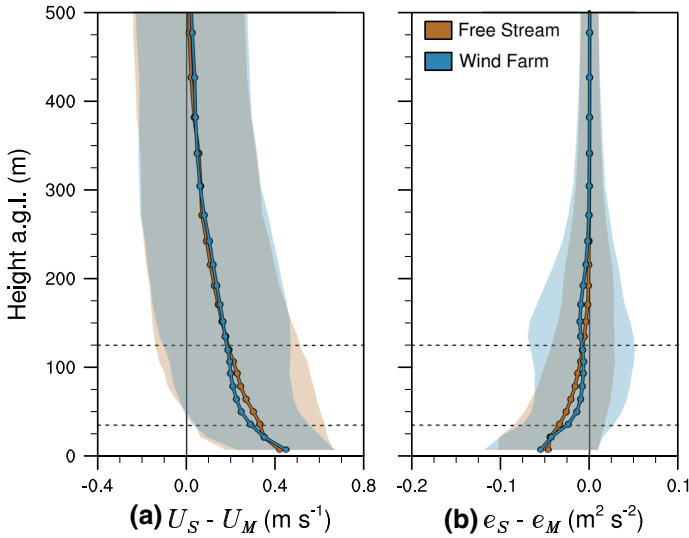


Fig. 5 Median profiles of the simulated **a** wind speed change (m s^{-1}) and **b** TKE (e) change ($\text{m}^2 \text{s}^{-2}$) resulting from a switch from maize to soybean surface roughness in the centre of the simulated wind farm. The comparison is shown for two freestream simulations (*brown*) and two simulations with a wind farm present (*turquoise*). Envelopes about the profiles represent the median absolute deviation. The *dashed lines* represent the turbine-rotor layer

the impact of roughness on both the magnitude of the wind speed and TKE (e) by $\approx 25\%$ in the bottom half of the rotor layer, declining to almost zero in the top half. The effects are a result of both the retardation of the flow and the increase in turbulent mixing caused by the simulated turbines. These processes are shown visually in Fig. 6, which features distributions of (a) the wind-speed change (m s^{-1}), and b TKE change ($\text{m}^2 \text{s}^{-2}$) caused by the addition of the wind farm in the maize surface set of simulations. Trends are indicated with respect to height and the 10–60 m bulk Richardson number, computed using

$$R_B = \frac{(g/T_v)\Delta\theta_v\Delta z}{(\Delta U)^2 + (\Delta V)^2}, \tag{1}$$

where g is the acceleration due to gravity, T_v is the average virtual temperature of the layer, $\Delta\theta_v$ is the difference in virtual potential temperature from the top of the layer to the bottom, Δz is the depth of the layer, and ΔU and ΔV are the differences in the zonal and meridional wind-speed components from the top of the layer to the bottom (Stull 1988). Larger positive values of R_B indicate increasing stability within the layer, while larger negative values indicate increasing instability.

The effects of the wind farm are most pronounced for stable conditions (values of R_B between 0.05 and 0.3): an approximate 2 m s^{-1} wind-speed decrease and $1 \text{ m}^2 \text{ s}^{-2}$ TKE (e) increase. Rotor-layer changes in wind speed and TKE (e) are statistically significant for *all* displayed R_B values according to the non-parametric Wilcoxon signed-rank test with $p = 0.95$ (Wilks 2011). Lack of significance is indicated by the hatched areas. In general, increasing instability tends to disperse the effects of the wind turbines throughout a deep layer from the surface to 300–400 m above the ground, as would be expected in the presence of strong convective plumes. Meanwhile, increasing stability constrains wind-speed decreases and TKE (e) increases into ever-smaller layers centred on the upper half of the rotor disk.

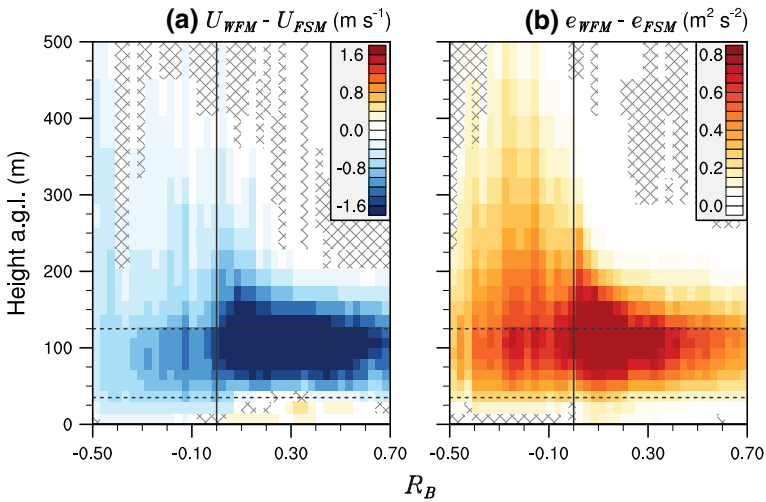


Fig. 6 Two-dimensional median distributions of the relationship between height, bulk Richardson number, and **a** wind-speed change (m s^{-1}) and **b** TKE (e) change ($\text{m}^2 \text{s}^{-2}$) resulting from the addition of the wind farm to the model grid with maize present. *Positive* values represent increases in the presence of the wind farm, while *negative* values represent decreases. *Hatched areas* illustrate regimes where the changes are not statistically significant according to the Wilcoxon signed-rank test at $p = 0.95$. *Dashed lines* indicate the turbine-rotor layer

These results agree with previous assessments of the interaction of elevated-drag WFPs (Fitch et al. 2013a, b) with variations in stability.

The differences between the freestream and wind-farm results follow from the functional effects of the wind farm presented in Fig. 6. The wind-speed increases resulting from the use of soybeans enable increased momentum extraction by the wind farm (and therefore increased power generation). Additionally, turbulence generation by the wind farm increases vertical momentum fluxes near the rotor layer, which mixes surface effects throughout a deeper vertical layer. The two mechanisms combine to dampen the crop effect on wind speeds in the rotor layer specifically. Ultimately, these differences between the freestream and wind-farm simulation suites are small and well within the sample uncertainty for each profile. There exists some debate as to whether elevated-drag parametrizations should explicitly add TKE (e.g., Jacobson and Archer 2012 assume implicit TKE generation). However, any hypothetical overestimation of TKE by the WRF-WFP model would only reduce the difference between the freestream and wind-farm results. Therefore, in the interest of brevity, all results hereafter utilize the simulations with the wind farm present.

The effect of crop roughness on rotor-layer wind speeds (Fig. 7) is much smaller than the effect of adding the wind farm to the maize simulation (Fig. 6). However, note that for all but the most stable R_B regimes, rotor-layer wind-speed differences between the maize and soybean simulations are statistically significant, even in the presence of the wind farm. These differences are a maximum in convective conditions, where maize-to-soybean wind-speed increases exceed 0.4 m s^{-1} . This wind-speed impact is lofted by vigorous convective plumes, with significant differences extending up to 500 m. Meanwhile, when the boundary layer is very stable, the roughness effect is confined to a small layer within the first 20 m above the surface (Mahrt 1999). These results illustrate the importance of boundary-layer stability to crop-turbine interactions, which is comparable to the observed influence of stability on wind-turbine performance (Wharton and Lundquist 2012; Vanderwende and Lundquist 2012).

Fig. 7 A two-dimensional median distribution of height, bulk Richardson number, and the wind-speed change (m s^{-1}) resulting from a switch from maize to soybean surface roughness in the centre of the simulated wind farm. *Hatched areas* illustrate regimes where the changes are not statistically significant according to the Wilcoxon signed-rank test at $p = 0.95$. *Dashed lines* indicate the turbine-rotor layer

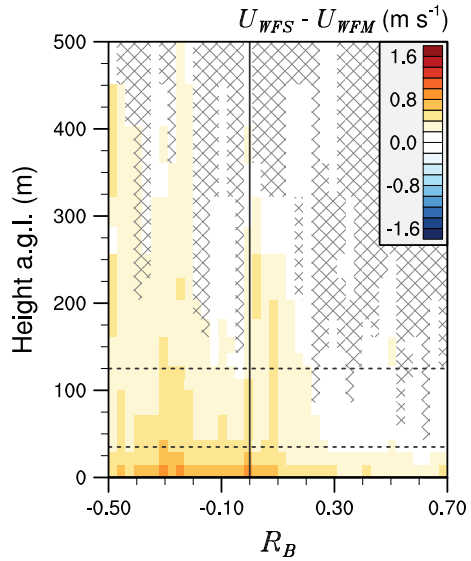


Table 2 Ranges of bulk Richardson number (R_B) encompassed by the four defined stability classes

Stability classes	Ranges	Occurrences
Convective (unstable)	$R_B < -0.05$	1536 (34 %)
Near-neutral	$-0.05 \leq R_B < 0.05$	565 (13 %)
Stable	$0.05 \leq R_B < 0.3$	1465 (33 %)
Very stable	$0.3 \leq R_B$	899 (20 %)

Also provided is the number of times each stability class was simulated by the model at the wind farm

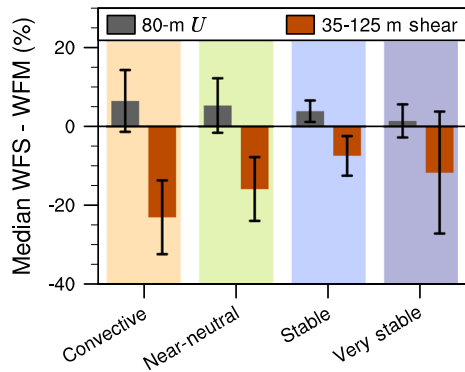
4 Impacts Across the Wind Farm in Various Stability Regimes

The results presented up to this point have illustrated the changes to the wind profile at one location within the wind farm. However, mesoscale weather fluctuations and terrain forcing on the flow can induce variability in the wind field throughout the turbine array. Therefore, in this section, we analyze the impacts across the whole wind farm of the change from maize to soybeans. To enable concise presentation of the data, we define four stability bins using ranges of R_B , which are summarized in Table 2 (along with number of occurrences in the simulation period). These bins are based on qualitative assessment of simulations as well as binning ranges used in prior analyses (Vanderwende and Lundquist 2012).

Median percentage changes in the 80-m (hub-height) wind speed and 35–125 m (rotor-layer) shear, computed using all 12 grid points within the wind farm for all time periods, are shown for the four stability classes in Fig. 8. Here, we represent shear by the power-law coefficient, often referred to as α , where the power law describes the relationship between wind speeds at two heights assuming that the profile can be represented adequately by a power law, it viz.,

$$u_2/u_1 = (z_2/z_1)^\alpha, \tag{2}$$

Fig. 8 Percentage changes in the 80-m wind speed (m s^{-1}) and 35–125 m wind shear resulting from a switch from maize to soybean surface roughness for the four defined stability regimes. Coloured bars represent medians over the spatial extent of the wind farm for the whole month, while black whiskers represent the median absolute deviations



where u_1 and u_2 represent the wind speeds at heights z_1 and z_2 , respectively. As the power law is simpler than the logarithmic-wind profile, it is often used in the wind industry to represent the rotor-layer shear (Peterson and Hennessey 1977). Values of α are known to vary considerably with boundary-layer stability (Walter et al. 2009).

The hub-height wind-speed increase produced by the switch from maize to soybeans is most strongly realized in convective (6.5%) and near-neutral conditions (5.5%). Stable conditions, which notably include the vast majority of LLJs, also yield significant wind-speed increases (3%). Only in very stable conditions, where surface drag influences do not penetrate to the rotor layer, do we see little hub-height wind-speed response.

The switch to soybeans reduces rotor-layer shear (α) for all stability classes, a result that is intuitive, since wind speeds are lowest near the surface. Therefore, if we preferentially increase wind speeds near the surface, low-level shear should decrease. Percentage changes in shear are large for convective (−23%) and near-neutral (−13%) conditions, though this result is mainly a consequence of the minimal shear present to begin with during those periods (shear is larger during stable conditions, and largest in very stable conditions Walter et al. 2009). Large reductions in shear were also produced for very stable conditions (−15%), mainly because wind speeds increase at 35 m, but the roughness effect is typically capped below 125 m. Therefore, shear throughout the rotor layer is reduced. Meanwhile, in stable conditions, enough mixing occurs to produce small wind-speed increases at 125 m, reducing the impact on rotor-layer shear (7.5%) compared to very stable periods. These reductions in shear (as with TKE) may improve turbine reliability, since high shear places a strain on the rotor through blade fluctuations out of the rotor plane (e.g., Eggers Jr et al. 2003).

The spatial variation of the crop effect in the stream-normal axis is surprisingly small across the roughness patch, as shown for each stability class in Fig. 9. For all time periods with a given stability class, a two-dimensional stream-normal slice centred on the middle of the wind farm is retrieved, and median percentage wind-speed changes are computed. Positive distances on the abscissa indicate downwind locations, while negative values represent those upwind; the extent of the roughness patch is indicated with vertical dashed lines. To avoid smearing of the roughness boundary due to the square shape of the patch, only wind directions within $\pm 10^\circ$ of north-east, south-east, south-west, and north-west directions are included in the median calculation.

The growth rate of the momentum IBL exhibits little sensitivity to the stability regime, although, stability strongly influences the eventual maximum height of the crop-change influence. These effects are capped in stable and very stable conditions to approximately 200 and 100 m above the ground, respectively, though small yet statistically significant wind-speed

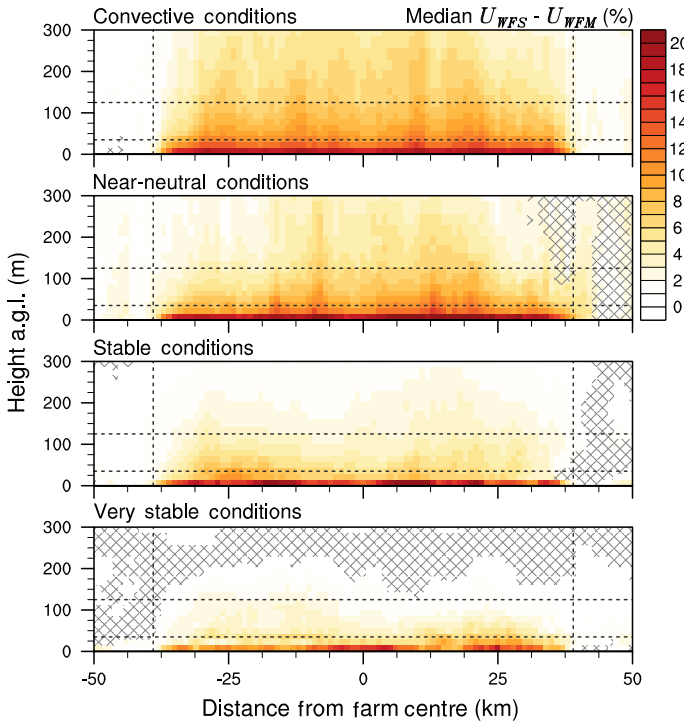
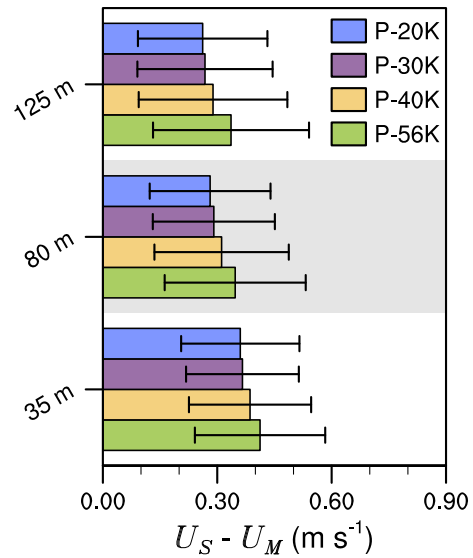


Fig. 9 Transects of the median wind-speed percentage change for the four defined stability regimes, following the inflow direction at the centre of the wind farm. *Negative* distances from the wind-farm centre represent upstream locations while *positive* values represent downstream locations. *Hatched areas* illustrate regions where the changes are not statistically significant according to the Wilcoxon signed-rank test at $p = 0.95$. *Horizontal dashed lines* indicate the turbine-rotor layer and the *vertical lines* the extent of the roughness patch. Wind directions within $\pm 10^\circ$ of north-east, south-east, south-west, and north-west are used to select only similar roughness fetches

increases do occur above these heights. For the most part, the growth of the IBL is much more rapid in the WRF model than predicted by the relationship in Mason (1988). Surface effects reach maximum magnitude throughout the rotor layer after only ≈ 13 -km fetch for all but near-neutral conditions, in which the IBL develops slowly and wind-speed changes maximize after a 50-km fetch. These results imply that a considerably smaller roughness patch could be used to achieve the same wind-speed gains in the rotor layer.

To evaluate the impact of patch size, we performed four additional simulations of a 1-week period (20–27 August 2013). In these model runs, we switch from maize to soybeans over progressively smaller patch sizes, ranging from the original 56.3² km² down to 20² km². In Fig. 10, we show that crop choices over patch sizes smaller than that derived from Mason (1988) still produce significant gains in hub-layer wind speeds. Even at the top of the rotor, where we expect fetch to matter most, reduction of the patch area, from 56.3² to 20² km², yields a wind-speed increase that is only 22% smaller than the original result. Some caution is advised, however, as studies have found the WRF model to produce unrealistically large vertical mixing (e.g., Cuxart and Holtslag 2006; Storm et al. 2010), which may explain some of the insensitivity of rotor-layer wind speed to patch size.

Fig. 10 Comparison of farm-averaged wind-speed differences over 1 week of August 2013, forced through the use of soybeans instead of maize across land areas of differing sizes. The *patch labels* indicate the length of one side of each *square patch* (i.e., *P-20K* indicates a patch with 20^2 km^2 area). *P-56K* patch matches the size of the original simulations presented in Figs. 5, 6, 7, 8 and 9



5 Estimating the Resulting Power Output and Economic Benefit

The statistically significant wind-speed impacts described in the previous sections demonstrate the potential benefits of targeted crop selection. However, the primary quantities of interest to wind-farm operators are the resultant power-output increase and possible economic gain. Wind-speed gains do not produce equivalent power gains due to the cubic dependence of power on wind speed and the shape of the turbine power curve (as in Fig. 2). A wind speed increase that occurs in the $6\text{--}10 \text{ m s}^{-1}$ range has a larger impact than one that occurs in the $10\text{--}12 \text{ m s}^{-1}$ range, and increases for wind speeds above 12 m s^{-1} have no impact at all. To determine the cumulative crop impact on power output for the hypothetical wind farm in August 2013, we use simulated wind speeds across the farm and the V90 power curve to compute the total wind-farm electrical production. Due to the use of the WFP, wake effects are included in the calculations presented here.

While hub-height wind-speed increases are largest (1.3 m s^{-1}) for hub-height wind speeds between 10 and 11 m s^{-1} , power output increases maximize (171 kW) between 9 and 10 m s^{-1} , as indicated by the distributions of both quantities in Fig. 11. Despite sizeable wind-speed increases below 4 m s^{-1} and above 11 m s^{-1} , little-to-no benefit in power output is simulated due to the shape of the power curve. If we sum the simulated power-output differences for the whole month of August 2013, we find that 4430 MWh of additional energy would be produced if soybeans replace maize. This increase represents nearly a 14% gain over the total energy produced in the maize simulation ($31,683 \text{ MWh}$). Assuming a typical market rate of US $\$30\text{--}60$ per MWh (Wiser and Bollinger 2014), the monetary benefit for the simulated wind farm may range from US $\$132,900$ to as much as US $\$265,800$ during August. Of course, this month typically features the maximum differences between the roughness effects of the crops.

Complicating matters is the persistent trend toward larger utility-scale turbines with higher hub heights and bigger rotor diameters (Wiser and Bollinger 2014). From Fig. 5, we see that sampling wind speed at greater heights reduces the impact of crop-roughness changes. In Fig. 12, we have quantified the maize-to-soybean roughness effect for a number of turbine

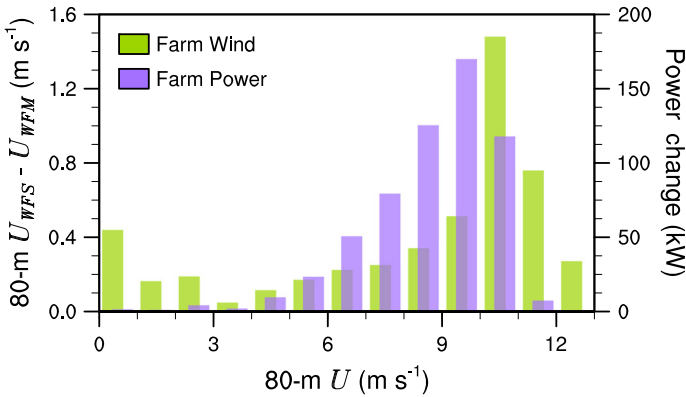


Fig. 11 Distributions of the simulated change in 80m wind speed (m s⁻¹) and the total farm power output (kW) for August 2013. Values are binned according to 80m inflow wind speeds (m s⁻¹)

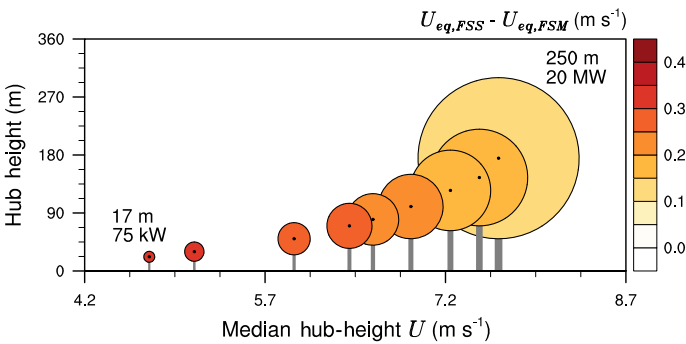


Fig. 12 The impact of switching from maize to soybean surface roughness on turbines with increasing hub heights and rotor diameters. The equivalent wind speed is used to quantify the wind-speed change (m s⁻¹). Turbines are organized along the *abscissa* according to the median inflow hub-height wind speed (m s⁻¹) experienced under simulated August 2013 conditions

sizes utilizing the equivalent wind speed (U_{eq}), a metric that represents the wind-speed profile across the rotor-disk in a single number (Antoniou et al. 2009; Wagner et al. 2009). As a result, the equivalent wind speed is more representative of the momentum available to the wind turbine than the hub-height wind speed during conditions with significant rotor-layer shear. The calculation of the equivalent wind speed is discussed in Appendix. Note that the equivalent wind speed does not account for rotor-layer wind veer, which can be significant in certain weather regimes (Walton et al. 2014; Vanderwende et al. 2015).

Increasing turbine sizes lessens the benefits of targeted crop selection, as seen in Fig. 12. Turbine hub heights and rotor diameters are visually represented by the scale rotor disks, shaded to represent the impact on the equivalent wind speed by the change in roughness from maize to soybeans. Turbine sizes range from a 17 m rotor-diameter 75 kW turbine to a hypothetical 250m rotor-diameter 20 MW turbine. These specifications match those used in Fig. 7.6 of the IPCC Special Report on Renewable Energy Sources and Climate Change Mitigation (2011). The shading represents the equivalent wind-speed gain (m s⁻¹) for each turbine, given August 2013 freestream conditions. These results indicate that present turbine-size trends tend to reduce the importance of the land surface in general.

6 Summary and Conclusions

The prevalence of wind energy in the agriculturally-productive US Midwest region motivated the study of simulated wind sensitivity to crop-induced roughness length changes at a location in central Iowa. We alter the surface roughness over a $56.3 \times 56.3 \text{ km}^2$ patch in the WRF model to represent, in four separate simulations, the influence of surface drag from a mature maize crop ($z_0 = 0.25 \text{ m}$) and a mature soybean crop ($z_0 = 0.1 \text{ m}$) during the month with the largest difference in crop heights. The simulations utilizing the soybean roughness produce increased hub-height wind speeds and decreased rotor-layer wind shear, even in the presence of an array of 121 Vestas V90 1.8-MW turbines. The additional mixing generated by the wind farm slightly reduces the effects of the crop roughness, but impacts on wind speed and shear are still statistically significant for all but the most stable conditions. Different atmospheric stability regimes imposed limits to the upper extent of the roughness impact, but had no consistent effect on the IBL growth rate.

Applying simulated wind-speed changes to the power curve of the V90 turbines produces a time series of total farm power output changes. These values, when summed over the entire month of August 2013, yield a 14% increase in energy production for the wind farm when the roughness patch consists of soy rather than maize. In terms of capacity factor for the wind farm, the crop switch produces an increase from 20 to 22%. Using typical market rates of US \$30–60 per MWh, the potential monetary gain ranges from US \$132,900 to US \$265,800. The results also suggest that a smaller roughness patch (as small as 20^2 km^2) could be used to produce similar results, increasing the practicality of the proposed crop management. However, the overly-diffusive nature of the WRF model must be considered when analyzing the upward propagation of the roughness forcing. If such vertical diffusion was sufficiently inflated by the model, our results presented herein would likely overstate the impact of the crop change. Finally, we assess how upward trends in turbine size would reduce the impact of crop-roughness changes.

These results hint at the possibility of improving wind-power yield in agriculturally-intensive regions through creative and coordinated crop management. Our findings also suggest the need for joint comparison of the roughness effects predicted by mesoscale numerical models and analytical models. The 14% power difference estimated here roughly matches that suggested by relationships derived for fully-developed wind-farm boundary layers (Meyers and Meneveau 2012), but such analytical models do not provide guidance on patch size requirements. Such models also assume neutrally-stratified conditions, which are ephemeral in the central USA.

Practical issues remain, such as the considerable spatial requirements of the roughness patch required to influence rotor-layer winds. Even the smaller patch size requirement suggested by the WRF model (20 km^2) is very large compared to the average size of a farm in Iowa, which was just above 1 km^2 in 2013 (US Department of Agriculture 2014). It is quite unlikely that such a large contiguous land area could be managed for the benefit of one wind farm. Additionally, crop choices are constrained by other factors such as market prices, soil conditions, and water availability. The significance of the potential economic benefit calculated herein would need to be weighed against these other considerations. Such analysis would be part of a thorough economic study, outside the scope of the present study.

Furthermore, to fully examine the potential impact of crop choices on wind-farm power output, simulations spanning the entire growth cycle with sophisticated representations of the time-varying roughness and moisture characteristics of the crops would be necessary. However, while theory from studies such as Mason (1988) suggest that crop selection over a large area should have an impact on rotor-layer winds, we demonstrate that the crop impact

persists despite varied meteorological conditions present in simulated real-world conditions. Our results illustrate the potential of coordination between farmers and wind-power producers, and demonstrate the need for more investigation into crop–turbine interaction.

Acknowledgments This work was supported by the National Renewable Energy Laboratory under APUP UGA-0-41026-22. CWEX is supported in part by the National Science Foundation under the State of Iowa EPSCoR Grant 1101284. We also highlight the generous support from National Science Foundation Grant BCS-1413980 (Coupled Human Natural Systems). We gratefully acknowledge the collaboration of Dr. Rod Linn and the Institutional Computing Program at the Los Alamos National Laboratory, who arranged for the computer time necessary for our simulations. We would also like to thank the Iowan farmers, specifically Mr. Russ Doorenbos, who provided insight into crop characteristics at the CWEX site. Finally, we thank our reviewers, whose insight motivated additional analysis into the impacts of patch size.

Open Access This article is distributed under the terms of the Creative Commons Attribution 4.0 International License (<http://creativecommons.org/licenses/by/4.0/>), which permits unrestricted use, distribution, and reproduction in any medium, provided you give appropriate credit to the original author(s) and the source, provide a link to the Creative Commons license, and indicate if changes were made.

Appendix

The equivalent wind speed, first discussed in Antoniou et al. (2009) and Wagner et al. (2009), represents the whole rotor-layer wind-speed profile with one concise value. This approach has multiple advantages over using the hub-height wind speed and a separate shear metric. It simplifies analysis of the wind resource, and can be used along with expected turbine-power curves to better predict power output for a given wind speed. The development of the metric was motivated in large part by recognition that the hub-height wind speed alone could not accurately predict power output in highly-sheared environments. Although the equivalent wind speed is a significant improvement over using hub-height wind speeds only, it still does not account for the effects of changes of wind direction with height on the turbine inflow.

Multiple discrete wind-speed values at different heights throughout the rotor layer are necessary to compute the equivalent wind speed. Here, we utilize those model levels that lie within the turbine–rotor disk, where the wind speed at each model level is weighted by the fraction of the rotor-disk area encompassed within that grid cell. Therefore, the equivalent wind speed (U_{eq}) is calculated from,

$$U_{eq} = \left(\sum_{i=1}^N u_i^3 \frac{A_i}{A} \right)^{1/3}, \tag{3}$$

where N is the number of model levels within the rotor layer, u_i and A_i are the wind speed and fractional area for the i th grid cell, respectively, and A is the total area of the rotor-disk. Each fractional area is assumed to be the sector of the rotor-disk circle bounded by the midpoints between the model levels above and below the i th level, assuming those midpoints also lie within the rotor-disk layer.

References

Adams AS, Keith DW (2013) Are global wind power resource estimates overstated? *Environ Res Lett* 8:015021
 American Wind Energy Association (2014) Iowa Wwind Energy, Washington, DC. <http://awea.files.cms-plus.com/FileDownloads/pdfs/Iowa.pdf>. Accessed 11 Nov 2014
 Antoniou I, Pedersen SM, Enevoldsen PB (2009) Wind shear and uncertainties in power curve measurement and wind resources. *Wind Eng* 33:449–468

- Baidya Roy S (2011) Simulating impacts of wind farms on local hydrometeorology. *J Wind Eng Ind Aerodyn* 99:491–498
- Baidya Roy S, Traiteur JJ (2010) Impacts of wind farms on surface air temperatures. *Proc Natl Acad Sci USA* 107:17899–17904
- Baidya Roy S, Pacala SW, Walko RL (2004) Can large wind farms affect local meteorology? *J Geophys Res* 109:D19101
- Barrie DB, Kirk-Davidoff DB (2010) Weather response to a large wind turbine array. *Atmos Chem Phys* 10:769–775
- Blahak U, Goretzki B, Meis J (2010) A simple parameterization of drag forces induced by large wind farms for numerical weather prediction models. In: *Proceedings of European wind energy conference and exhibition 2010*, Warsaw, Poland, pp 186–189
- Blom J, Wartena L (1969) The influence of changes in surface roughness on the development of the turbulent boundary layer in the lower layers of the atmosphere. *J Atmos Sci* 26:255–265
- Bonner WD (1968) Climatology of the low-level jet. *Mon Weather Rev* 96:833–850
- Bou-Zeid E, Meneveau C, Parlange MB (2004) Large-eddy simulation of neutral atmospheric boundary layer flow over heterogeneous surfaces: blending height and effective surface roughness. *Water Resour Res* 40:W02505
- Christiansen MB, Hasager CB (2005) Wake effects of large offshore wind farms identified from satellite SAR. *Remote Sens Environ* 98:251–268
- Claussen M (1990) Area-averaging of surface fluxes in a neutrally stratified, horizontally inhomogeneous atmospheric boundary layer. *Atmos Environ* 24:1349–1360
- Cuxart J, Holtslag AAM (2006) Single-column model intercomparison for a stably stratified atmospheric boundary layer. *Boundary-Layer Meteorol* 118:273–303
- Eggers AJ Jr, Digumarthi R, Chaney K (2003) Wind shear and turbulence effects on rotor fatigue and loads control. *J Sol Energy* 125:402–409
- Elliott WP (1958) The growth of the atmospheric internal boundary layer. *Eos Trans AGU* 39:1048–1054
- Fiedler F, Panofsky HA (1972) The geostrophic drag coefficient and the ‘effective’ roughness length. *Q J R Meteorol Soc* 98:213–220
- Fiedler BH, Bukovsky MS (2011) The effect of a giant wind farm on precipitation in a regional climate model. *Environ Res Lett* 6:045101
- Fitch AC, Olson JB, Lundquist JK, Dudhia J, Gupta AK, Michalakes J, Barstad I (2012) Local and mesoscale impacts of wind farms as parameterized in a mesoscale NWP model. *Mon Weather Rev* 140:3017–3038
- Fitch AC, Lundquist JK, Olson JB (2013a) Mesoscale influences of wind farms throughout a diurnal cycle. *Mon Weather Rev* 141:2173–2198
- Fitch AC, Olson JB, Lundquist JK (2013b) Parameterization of wind farms in climate models. *J Clim* 26:6439–6458
- Goode K, Belcher SE (1999) On the parameterisation of the effective roughness length for momentum transfer over heterogeneous terrain. *Boundary-Layer Meteorol* 93:133–154
- Hansen FV (1993) Surface roughness lengths. ARL technical report 88002-5501, White Sands Missile Range, 41 pp
- Harris RA, Zhou L, Xia G (2014) Satellite observations of wind farm impacts on nocturnal land surface temperature in Iowa. *Remote Sens* 6:12234–12246
- Hicks BB, Wesely ML (1981) Heat and momentum transfer characteristics of adjacent fields of soybeans and maize. *Boundary-Layer Meteorol* 20:175–185
- IPCC (2011) In: Edenhofer O, Pichs-Madruga R, Sokona Y, Seyboth K, Matschoss P, Kadner S, Zwickel T, Eickemeier P, Hansen G, Schlömer S, von Stechow C (eds) IPCC special report on renewable energy sources and climate change mitigation. Prepared by Working Group III of the Intergovernmental Panel on Climate Change. Cambridge University Press, Cambridge, 1075 pp
- Ivanova LA, Nadyozhina ED (2000) Numerical simulation of wind farm influence on wind flow. *Wind Eng* 24:257–269
- Jacobson MZ, Archer CL (2012) Saturation wind power potential and its implications for wind energy. *Proc Natl Acad Sci USA* 109:15679–15684
- Jiménez PA, Javaro J, Palomares AM, Dudhia J (2014) Mesoscale modeling of offshore wind turbine wakes at the wind farm resolving scale: a composite-based analysis with the Weather Research and Forecasting model over Horns Rev. *Wind Energy* 18:559–566
- Keith D, DeCarolis J, Denkenberger D, Lenschow D, Malyshev S, Pacala S, Rasch PJ (2004) The influence of large-scale wind power on global climate. *Proc Natl Acad Sci USA* 101:16115–16120
- Kelley ND (2011) Turbulence–turbine interaction: the basis for the development of the TurbSim stochastic simulator. Technical report EL-500-29798, 332 pp

- Kirk-Davidoff DB, Keith DW (2008) On the climate impact of surface roughness anomalies. *J Atmos Sci* 65:2215–2234
- Lundquist JK, Takle ES, Boquet M, Kosović B, Rhodes ME, Rajewski D, Doorenbos R, Irvin S, Aitken ML, Friedrich K, Quelet PT, Rana J, St. Martin C, Vanderwende B, Worsnop R (2014) Lidar observations of interacting wind turbine wakes in an onshore wind farm. In: EWEA 2014, Barcelona. <http://www.leosphere.com/wp-content/uploads/2014/04/Lidar-observations-of-interacting-wind-turbine.pdf>. Accessed 23 Jan 2015
- Mahrt L (1999) Stratified atmospheric boundary layers. *Boundary-Layer Meteorol* 90:375–396
- Mason PJ (1988) The formation of areally-averaged roughness lengths. *Q J R Meteorol Soc* 114:399–420
- Meyers J, Meneveau C (2012) Optimal turbine spacing in fully developed wind farm boundary layers. *Wind Energy* 15:305–317
- Panofsky HA, Townsend AA (1964) Change of terrain roughness and the wind profile. *Q J R Meteorol Soc* 90:147–155
- Peterson EW (1969) Modification of mean flow and turbulent energy by a change in surface roughness under conditions of neutral stability. *Q J R Meteorol Soc* 95:561–575
- Peterson EW, Hennessey JP (1977) On the use of power laws for estimates of wind power potential. *J Appl Meteorol* 17:390–394
- Rajewski D, Takle G, Lundquist JK, Rhodes ME, Oncley S, Horst T (2013) Crop wind energy experiment (CWEX): observations of surface-layer, boundary layer, and mesoscale interactions with a wind farm. *Bull Am Meteorol Soc* 94:655–672
- Rhodes ME, Lundquist JK (2013) The effect of wind-turbine wakes on summertime US Midwest atmospheric wind profiles as observed with ground-based doppler lidar. *Boundary-Layer Meteorol* 149:85–103
- Skamarock WC, Klemp JB, Dudhia J, Gill DO, Barker DM, Duda MG, Huang X, Wang W, Powers JG (2008) A description of the advanced research WRF version 3. NCAR technical note NCAR/TN-475+STR, 125 pp
- Storm B, Dudhia J, Basu S, Swift A, Giammanco I (2010) Evaluation of the weather research and forecasting model on forecasting low-level jets: implications for wind energy. *Wind Energy* 12:81–90
- Stull RB (1988) An introduction to boundary layer meteorology. Kluwer Academic Publishers, Dordrecht, 670 pp
- Townsend AA (1965) The response of a turbulent boundary layer to abrupt changes in surface conditions. *J Fluid Mech* 22:799–822
- US Department of Agriculture, National Agricultural Statistics Service (2014) Farms, land in farms, and livestock operations 2013 summary. US Department of Agriculture, Washington, DC. <http://usda.mannlib.cornell.edu/usda/current/FarmLandIn/FarmLandIn-05-28-2014.pdf>. Accessed 11 Nov 2014
- US Department of Energy, Office of Energy Efficiency and Renewable Energy (2008) 20% Wind energy by 2030: increasing wind energy's contribution to U.S. electricity supply. NREL report number TP-500-41869 DOE/GO-102008-2567. US Department of Energy, Washington, DC. <http://www.nrel.gov/docs/fy08osti/41869.pdf>. Accessed 11 Nov 2014
- Vanderwende BJ, Lundquist JK (2012) The modification of wind turbine performance by statistically distinct atmospheric regimes. *Environ Res Lett* 7:034035
- Vanderwende BJ, Lundquist JK, Rhodes ME, Takle ES, Irvin SL (2015) Observing and simulating the summertime low-level jet in central Iowa. *Mon Weather Rev* 143:2319–2336
- Vautard R, Thais F, Tobin I, Bréon F-M, Devezeaux de Lavergne J-G, Colette A, Yiou P, Ruti PM (2014) Regional climate model simulations indicate limited climatic impacts by operational and planned European wind farms. *Nat Commun* 5:3196
- Wagner R, Antoniou I, Pedersen SM, Courtney MS, Jørgensen HE (2009) The influence of the wind speed profile on wind turbine performance measurements. *Wind Energy* 12:348–362
- Walter K, Weiss CC, Swift AH, Chapman J, Kelley ND (2009) Speed and direction shear in the stable nocturnal boundary layer. *J Sol Energy Eng* 131:011013
- Walton RA, Takle ES, Gallus WA Jr (2014) Characteristics of 50–200 m winds and temperatures derived from an Iowa tall tower network. *J Appl Meteorol Climatol* 53:2387–2393
- Wang C, Prinn RG (2010) Potential climatic impacts and reliability of very large-scale wind farms. *Atmos Chem Phys* 10:2053–2061
- Wang C, Prinn RG (2011) Potential climatic impacts and reliability of large-scale offshore wind farms. *Environ Res Lett* 6:025101
- Wharton S, Lundquist JK (2012) Atmospheric stability affects wind turbine power collection. *Environ Res Lett* 7:014005
- Wieringa J (1976) An objective exposure correction method for average wind speeds measured at a sheltered location. *Q J R Meteorol Soc* 102:241–253
- Wieringa J (1992) Updating the Davenport roughness classification. *J Wind Eng Ind Aerodyn* 41:357–368

- Wieringa J (1993) Representative roughness parameters for homogeneous terrain. *Boundary-Layer Meteorol* 63:323–363
- Wilks DS (2011) *Statistical methods in the atmospheric sciences*. Academic Publishers, Oxford, 704 pp
- Wiser R, Bollinger M (2014) 2013 Wind technologies market report. US Department of Energy, Washington, DC, 82 pp
- Zhou L, Tian Y, Baidya-Roy S, Thorncroft C, Bosart LF, Hu Y (2012) Impacts of wind farms on land surface temperature. *Nat Clim Change* 2:539–543